Combustion and Flame 274 (2025) 113993

Contents lists available at ScienceDirect

Combustion and Flame

journal homepage: www.sciencedirect.com/journal/combustion-and-flame

Computational diagnostics and characterization of combustion recession in diesel sprays

F.J. Arguelles [a], M.D. Fagade [a], J. Mehra [a], C. Xu [b], N. Sekularac [c], X.H. Fang [a,*]

[a] Department of Mechanical and Manufacturing Engineering, University of Calgary, 2500 University Drive NW, Calgary, AB T2N 1N4, Canada
[b] Transportation and Power Systems Division, Argonne National Laboratory, 9700 S. Cass Avenue, Lemont, IL 60439, USA
[c] CERFACS, 42 Avenue Gaspard Coriolis, 31057 Toulouse, France

ARTICLE INFO

Keywords:
Combustion recession
"Spray A"
CEMA
Combustion recession metric
Large eddy simulations

ABSTRACT

While low-temperature combustion (LTC) strategies have been found to mitigate nitrogen oxides and particulate matter emissions in diesel engines, studies have also associated LTC with an increase in unburnt hydrocarbons. With more recent studies on diesel after end-of-injection (AEOI), combustion recession is identified as a phenomenon where at near nozzle region, high-temperature ignition (HTI) combustion can propagate back to the nozzle tip consuming the unburnt hydrocarbons AEOI. Current literature has suggested that combustion recession is controlled by auto-ignition. However, high-fidelity simulations and detailed analysis of such a mechanism are missing. In this study, comprehensive Large Eddy Simulations of a reacting spray at "Spray A" conditions are performed, where detailed analysis of combustion recession concerning flame morphology and propagation modes are included. In particular, this study demonstrated for the first time that while combustion recession is mainly auto-ignition dominated (consistent with the literature), a cool flame was found to deflagrate towards the richer regions of the mixture, promoting mixing and increasing the mixture temperature. This leads to HTI kernels, which then grow and develop as deflagrative waves, therefore sustaining the combustion recession process. The study also detailed the extinction mechanism of combustion: the entrainment wave will overlean the near-nozzle mixtures, rendering it unable to support HTI, which leads to the extinction of the upstream flame AEOI in lower reactivity mixtures. Combustion recession is also observed to be contingent on the chemical and diffusion processes, even at low scalar dissipation rates. Finally, a new criterion for combustion recession based on chemical explosive mode is proposed and validated with previous combustion recession index to quantify the extent of HTI in near-nozzle mixtures AEOI. The newly developed metric combined with a previous experimentally-based metric can provide simple but valuable measurements of the degree and propensity of the upstream flame AEOI.

Novelty and Significance Statement

This work covers the literature gap in detailing the spray after end-of-injection combustion recession mechanisms. The study is significant, suggesting that while combustion recession is auto-ignition-dominated, deflagration modes were found, for the first time, to exist within the kernels via a cool flame at the end of injection. With further analysis, the deflagration modes were found to promote mixing at the end of injection which is deemed critical in sustaining combustion recession. The extinction mechanisms on the other hand were associated with the significant role of entrainment waves after end-of-injection. To generalize the findings of our study, a novel combustion recession metric based on the chemical explosive mode is proposed where agreement is found with the experimental observations. The new metric can provide an effective computational diagnostics tool for 3-D numerical simulations which complements the previous experimental metric in identifying the propensity and degree of combustion recession.

1. Introduction

Diesel engines are efficient, reliable, and durable, making them a popular choice for everyday transportation and heavy-duty commercial applications. However, with ever-increasing environmental regulations and restrictions, their nitrogen oxide (NOx) and particulate matter (PM) emissions pose a significant challenge to their feasibility. To maintain the competitiveness of diesel engines in the foreseeable future, more advanced combustion strategies must be developed and implemented

* Corresponding author.
E-mail address: xiaohang.fang@ucalgary.ca (X.H. Fang).

https://doi.org/10.1016/j.combustflame.2025.113993
Received 30 July 2024; Received in revised form 30 October 2024; Accepted 17 January 2025
Available online 5 February 2025

to reduce these emissions. Low-temperature combustion (LTC) is a strategy that decreases the mixture temperatures within the cylinder and increases the overall air-fuel mixing [1]. This strategy typically incorporates exhaust gas recirculation, a technique in which part of the exhaust gas is recirculated back into the cylinders and mixed with the fresh mixture, thereby reducing the in-cylinder temperatures and increasing overall mixing [1]. Previous studies [2–5] have shown that the LTC strategy can significantly reduce NOx and PM emissions in modern diesel engines. However, unburned hydrocarbon (UHC) emissions can also increase with LTC [1]. Thus, a more in-depth characterization of LTC diesel sprays is needed to improve the understanding of the underlying processes contributing to the increased UHC emissions.

While various studies [6–8] have shown that start-of-injection (SOI) processes can significantly impact NOx and PM formation, end-of-injection (EOI) processes have also been demonstrated to play an important role in UHC emissions formation in LTC diesel engines [9–11]. Specifically, Musculus et al. [9] observed that after EOI (AEOI), mixtures near the nozzle gradually become leaner. In a later study [12], they developed a 1-D diesel jet model to understand the mixing process behind this behavior and found that an entrainment wave occurs AEOI. Entrainment waves are a mixture of air, fuel, and combustion products that travels upstream, which in turn leans the mixtures near the nozzle [12]. The study also found that a faster injection rate ramp-down resulted in a stronger entrainment wave and increased UHC emissions. To mitigate the increase in UHCs, a different study by Knox et al. [13] controlled the injection rate ramp-down and observed that AEOI, high-temperature ignition (HTI) occurred near the injector nozzle, named combustion recession. Combustion recession is an EOI phenomenon where HTI occurs upstream of the flame lift-off length (FLOL) AEOI, consuming UHCs in the process. It should be noted that this is not the same phenomenon as flashback, where the flame propagates back towards the fuel nozzle due to a discrepancy between the local flame speed and the velocity of the fuel jet [9]. Instead, current literature [14–17] suggests that combustion recession is likely attributed to auto-ignition.

As one of the earliest experimental studies on combustion recession, Koci et al. [16] examined the effects of the ramp-down rate on combustion recession. The study differentiated two types of combustion recession: strong combustion recession, a complete recession of electronically excited forms of the hydroxyl radical (OH*) and the methylidyne radical (CH*) chemiluminescence towards the injector nozzle, and weak combustion recession, a partial recession of OH* chemiluminescence towards the injector nozzle with no CH* chemiluminescence [16]. The strong combustion recession occurred at slower ramp-down rates, higher ambient temperatures, and higher oxygen concentrations, whereas the weak combustion recession occurred at faster ramp-down rates with lower ambient temperatures and oxygen concentrations [16]. They also found that decreasing the ambient temperature changed the behavior of combustion recession from a continuous stream of ignition to separate ignition kernels, suggesting that combustion recession is dominated by auto-ignition rather than deflagration [16]. Similar results were found in the work of Knox et al. [17] by decreasing ambient temperatures and oxygen concentrations. Although the aforementioned studies provided experimental evidence on the different types of combustion recession, numerical simulations can further provide fundamental understanding of combustion recession while also complementing the experimental findings.

In a numerical study of combustion recession, Jarrahbashi et al. [14] performed a 3-D reacting spray simulation using the Reynolds-Averaged Navier–Stokes (RANS) framework and two reduced chemical kinetic mechanisms for n-dodecane developed by Cai et al. [18] and Yao et al. [19]. (Note: for the sake of brevity, the chemical mechanisms will henceforth be referred to as the "[first author] mechanism" throughout the rest of this study). The study simulated a reacting spray using the Engine Combustion Network's (ECN) "Spray A" condition [20]. The "Spray A" condition is a set of boundary conditions that emulates LTC of diesel with exhaust gas recirculation [20]. With ambient temperatures of 800 K and 900 K, combustion recession was found to occur as separate ignition kernels, where the kernels were smaller under the 800 K condition than the 900 K condition [14]. With an ambient temperature of 1000 K, combustion recession did not appear as separate kernels, but as a continuous stream of ignition upstream of the FLOL [14]. In another RANS study, Jarrahbashi et al. [21] analyzed the effects of EOI transients on combustion recession and found that fast ramp-down rates suppressed combustion recession while combustion recession was present during slower ramp-down rates. The fast ramp-down rates resulted in a faster and larger entrainment wave towards the nozzle, where the entrainment wave overleans the mixture, preventing HTI [12,21]. These earlier numerical studies have proven that numerical simulations can predict combustion recession, yielding similar results to the experimental findings mentioned earlier.

Following these early studies on combustion recession, subsequent numerical studies have been focused on improving the modeling capabilities to better predict combustion recession and its characteristics. Employing "Spray A" conditions, Fang et al. [22] tested the effects of different combustion models on combustion recession including a finite rate chemistry model SAGE [23], Representative Interactive Flamelet [24], and Flame Generated Manifold (FGM) [25]. Overall, they found that all combustion models were able to predict combustion recession with satisfactory precision [22]. In particular, using FGM and the Cai and Yao mechanisms (which account for LTC), the authors highlighted how low-temperature chemistry affects the HTI upstream of the FLOL AEOI [22]. In another study performed by Fang et al. [26], they compared two RANS-FGM models using chemistry manifolds obtained from 0-D igniting homogeneous reactors and 1-D igniting counterflow diffusion flames to predict combustion recession, respectively. Although both approaches were able to qualitatively capture the quasi-steady flame structure, using the homogeneous reactor-based manifold failed to predict combustion recession due to the lack of diffusive transport effects within the manifold, emphasizing that diffusion processes play a role in predicting HTI AEOI [26]. They also investigated the effect of the chemical kinetics on combustion recession predictions using Cai, Yao, Luo [27], and Ranzi [28] mechanisms. Compared to the other three chemical mechanisms, the Yao mechanism predicted the furthest combustion recession phenomenon due to its high chemical source term in the ignition region, supporting previous experimental observations that combustion recession is auto-ignition dominated. In yet another study, Fang et al. [29] utilized the Conditional Source-term Estimation model [30] coupled with FGM to simulate LTC diesel sprays and found that it was capable of accurately predicting the complex spray combustion processes. In a subsequent parametric study using the same model Fang et al. [31], varied the ambient temperatures (800 K, 900 K, and 1100 K) and oxygen concentrations (13%, 15%, and 21% by volume) in the "Spray A" conditions. Similar to previous experimental results [15,17], they found combustion recession to occur at higher ambient temperatures and higher oxygen concentrations.

While the parametric studies mentioned above have provided new insights into the propensity of combustion recession under varying conditions, most of these studies employed RANS simulations, which might overlook finer details of the physical phenomena. While Direct Numerical Simulations (DNS) can fully resolve the flow field, they are still computationally prohibitive. Thus, Large Eddy Simulations (LES), which resolve large-scale flows and model the smaller ones, can provide finer details in the flow while being computationally viable [32]. In a recent LES study by Zhang et al. [33], combustion recession both occurred using 90 μm ("Spray A") and 186 μm ("Spray D") diameter nozzles, albeit in different forms. "Spray A" resulted in separate ignition kernels, while "Spray D" resulted in a continuous ignition stream upstream of the FLOL [33]. Moreover, a similar study by Zhang et al. [34] found that combustion recession occurs at lower

ambient temperatures (800 K), but only with a lower prescribed injection pressure of 50 MPa. This is because higher injection pressures increase entrainment AEOI, which causes the mixture to become overly lean, resulting in inadequate thermodynamic conditions for combustion recession to occur [34].

The previous experimental and numerical studies on diesel spray combustion AEOI at LTC conditions provided a foundation for the characterization of combustion recession. These studies found that combustion recession occurs either as a continuous stream of ignition or separate ignition kernels propagating towards the injector nozzle. In addition, combustion recession is affected by ambient conditions, such as temperature and oxygen concentration, and injector conditions such as injection pressure. A common consensus from these studies is that combustion recession is mainly attributed to auto-ignition modes rather than deflagration modes. To substantiate this idea, computational diagnostics of the reacting spray may be beneficial to help understand the flame characteristics, such as stabilization and propagation, AEOI.

Therefore, the objective of this study lies in conducting high-fidelity LES at LTC conditions in order to capture and analyze combustion recession. To achieve this objective, a computational diagnostic tool, Chemical Explosive Mode Analysis (CEMA), is implemented to study the EOI combustion modes near the injector nozzle. The target condition is "Spray A" with variations in ambient temperature, oxygen concentration, and injection pressure to understand their effects on the combustion mode of the near-nozzle mixtures.

2. Methodology

2.1. Computational setup

The numerical simulations are carried out using the CONVERGE CFD solver in an Eulerian–Lagrangian framework, distributing mass, momentum, and energy source terms from the liquid phase to the nearest nodes in the Eulerian gas phase. Turbulence is modeled with LES using the one-equation viscosity model formulated by Yoshizawa & Horiuti [35] and Menon et al. [36]. Fig. 1 illustrates the computational domain. Similar to the combustion chamber used in the experiments, the simulations were performed in a cylindrical chamber with a diameter of 54 mm and a height of 100 mm, where the injector nozzle tip, denoted by a green X marker in Fig. 1, is located at one end of the cylinder along the center line. (Note: the axial (x) and radial (y) positions of 0 mm correspond to the location of the injector nozzle tip). Fixed embedding in a volume with an initial radius of 1 mm, a final radius of 2 mm, and a length of 7 mm along the nozzle tip is implemented, depicted by the solid blue lines in Fig. 1. This is to increase the accuracy of the high-velocity liquid spray region as the flame behavior is affected by the spray evolution. Adaptive mesh refinement is also implemented in the whole domain to refine cells up to 4 embedding levels based on subgrid velocity and temperature fluctuations to increase the overall accuracy of the reacting spray. A base grid resolution with a base grid size of 1 mm and a minimum grid size of 62.5 μm are used, which have been tested and employed in previous numerical simulations [37,38] that successfully simulated the reacting "Spray A" conditions. To further improve the accuracy of combustion recession, simulations employing a refined grid resolution are also performed. The fixed embedding level in this resolution is increased by one, resulting in a minimum grid size of 31.25 μm near the nozzle. The Luo and Yao mechanisms are employed as they were developed to account for diesel spray LTC [19,27]. In particular, the Yao mechanism was specifically adopted for "Spray A" applications [19].

The injected droplets are set equal to the effective nozzle diameter [39]. The modified Kelvin–Helmholtz Rayleigh–Taylor model [40] is used to simulate the droplet breakup. The No-Time-Counter model [41] is used to simulate droplet collision. The Frossling correlation [42] is used to model droplet evaporation. The dynamic drag model [43], the O'Rourke model [42], and the wall impingement model [44,45] are used to model the drop drag, drop turbulent dispersion, and drop/wall interaction, respectively. The sub-models outlined above have been adopted from Fang et al.'s previous studies where the details are available [22,26,29,31]. In this study, SAGE, a well-stirred reactor (WSR) model, is used to model combustion. In WSR models, each cell is assumed to be homogeneous, and the mean reaction rates are calculated with the Arrhenius equations. Consequently, SAGE can potentially result in large errors as it ignores turbulence-chemistry interaction effects; however, this error can be substantially reduced by increasing the grid resolution [46]. In studies by Pei et al. [47,48], the authors utilized SAGE to simulate a reacting spray flame under "Spray A" conditions. They found that either a minimum grid size smaller than the nozzle diameter or 62.5 μm led to grid-convergent results that are comparable to experimental data [47,48] and simulations incorporating a combustion model with turbulence-chemistry interactions [49]. Considering that the minimum grid size in this study is less than or equal to 62.5 μm, SAGE can effectively and accurately model the reacting spray and subsequently the combustion recession. However, the authors acknowledge that turbulence-chemistry interaction models are needed to adequately capture the effects of heterogeneity within the subgrid scales [50].

Table 1
The boundary conditions investigated in this study. The baseline condition is denoted by bold text.

Parameter	Values
Ambient temperature (K)	800, **900**, 1000
Ambient pressure (MPa)	5.25, **6.09**, 6.62
Ambient oxygen concentration (% O_2 by volume)	13, **15**, 21, 0 (non-reacting)
Injection pressure (MPa)	50, **150**
Injection mass (mg)	6.95, **3.46**
Injection duration (ms)	5.65, **1.54**

The boundary conditions, based on the ECN's "Spray A" conditions, are summarized in Table 1. (Note: the numerical simulations will only have one parametric variation from the baseline condition and will generally be referred to as the [parametric variation] case, e.g. 1000 K case). The surrogate fuel is *n*-dodecane (n-$C_{12}H_{26}$) with an injection temperature of 363 K and a density of 689 kg/m^3. The fuel is injected into the cylindrical combustion chamber from a single-hole axial injector nozzle that has an outlet diameter of 90 μm. The variations of ambient temperature, oxygen concentration, and injection pressure are examined to see their effects on combustion recession. The ambient pressure is adjusted when the ambient temperature is changed as the ambient density is kept constant. The injection mass and duration are also corrected when the injection pressure is changed to better match previous experimental conditions.

2.2. Chemical explosive mode analysis

CEMA [51] is a computational diagnostic tool based on the eigenanalysis of the chemical Jacobian to identify flame limit phenomena. The governing equation in the Lagrangian system for a typical reacting flow is defined as:

$$\frac{D\boldsymbol{y}}{Dt} = \boldsymbol{\omega}(\boldsymbol{y}) + \boldsymbol{s}(\boldsymbol{y}), \tag{1}$$

where $\boldsymbol{y}$ is the vector form of dependent variables, including temperature and species concentrations, $\boldsymbol{\omega}$ represents the chemical source term, and $\boldsymbol{s}$ represents the non-chemical source terms, such as diffusion and mixing, associated with the system. The dynamics of $\boldsymbol{\omega}$ can be determined using the chain rule, resulting in:

$$\frac{D\boldsymbol{\omega}(\boldsymbol{y})}{Dt} = \boldsymbol{J}_{\boldsymbol{\omega}}\frac{D\boldsymbol{y}}{Dt} = \boldsymbol{J}_{\boldsymbol{\omega}}(\boldsymbol{\omega}+\boldsymbol{s}), \boldsymbol{J}_{\boldsymbol{\omega}} = \frac{\partial\boldsymbol{\omega}}{\partial\boldsymbol{y}}, \tag{2}$$

where $\boldsymbol{J}_{\boldsymbol{\omega}}$ is the chemical Jacobian. It should be noted that a separate chemical Jacobian is calculated for each chemical mechanism due to a difference in species and reactions. A chemical explosive mode (CEM)

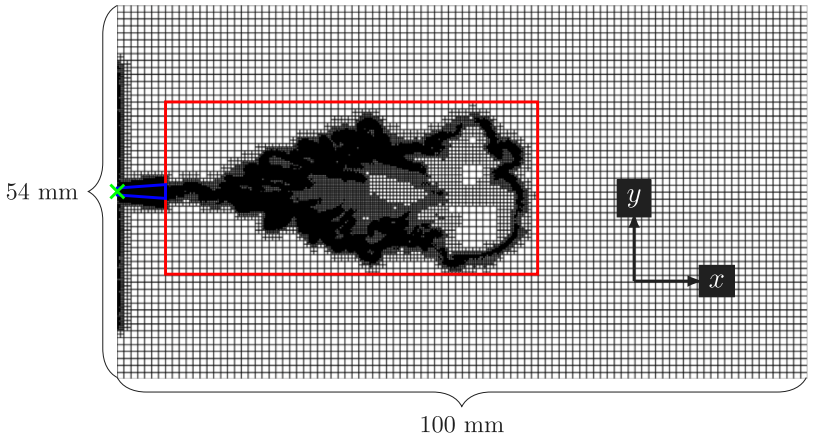

Fig. 1. The computational domain with a base grid size of 1 mm. The blue area denotes where fixed embedding is implemented. The red area denotes the spray area where adaptive mesh refinement refined the grid. The green X marker denotes the injector nozzle location. (For interpretation of the references to color in this figure legend, the reader is referred to the web version of this article.)

Table 2
CEMA criteria for local combustion modes.

Criterion	$\alpha < -1$	$-1 \leq \alpha \leq 1$	$\alpha > 1$
$\lambda_e < 0$	Non-explosive	Non-explosive	Non-explosive
$0 \leq \lambda_e \leq 1$	Non-reactive	Non-reactive	Non-reactive
$\lambda_e > 1$	Extinction	Auto-ignition	Deflagration

is defined as an eigenmode associated with a real positive eigenvalue, λ_e:

$$\lambda_e = \boldsymbol{b}_e \cdot \boldsymbol{J}_{\boldsymbol{\omega}} \cdot \boldsymbol{a}_e, \tag{3}$$

where $\boldsymbol{a}_e$ and $\boldsymbol{b}_e$ are the right and left eigenvectors, respectively. λ_e refers to the eigenvalue of the fastest CEM as ignition processes are mostly controlled by the fastest CEM [52]. λ_e also refers to the real part of the largest non-conservative eigenvalue if no CEM is present. By definition, CEM is purely a chemical property, and can interact with other physical processes such as diffusion, evaporation, radiation, etc. [53].

To identify different combustion modes, Xu et al. [52] projected Eq. (2) to the CEM:

$$\boldsymbol{b}_e \cdot \frac{\mathrm{D}\boldsymbol{\omega}(\boldsymbol{y})}{\mathrm{D}t} = \boldsymbol{b}_e \cdot \boldsymbol{J}_{\boldsymbol{\omega}}(\boldsymbol{\omega} + \boldsymbol{s}) = \lambda_e \boldsymbol{b}_e \cdot (\boldsymbol{\omega} + \boldsymbol{s}), \tag{4}$$

$$\frac{\mathrm{D}\phi_{\boldsymbol{\omega}}}{\mathrm{D}t} = \lambda_e \phi_{\boldsymbol{\omega}} + \lambda_e \phi_s + \frac{\mathrm{D}\boldsymbol{b}_e}{\mathrm{D}t} \cdot \boldsymbol{\omega}, \tag{5}$$

$$\phi_\omega = \boldsymbol{b}_e \cdot \boldsymbol{\omega}, \phi_s = \boldsymbol{b}_e \cdot \boldsymbol{s}, \tag{6}$$

where $\phi_{\boldsymbol{\omega}}$ and ϕ_s are the projected chemical and diffusion source terms, respectively. The last term in Eq. (5) represents a non-linear effect induced by the rotation of the eigenvector [52], which is ignored in this study. Xu et al. [52] further defined a local combustion mode indicator, α:

$$\alpha = \frac{\phi_s}{\phi_{\boldsymbol{\omega}}}, \tag{7}$$

which indicates the relative importance of chemistry and diffusion in the combustion process [52]. Table 2 outlines the different local combustion modes from CEMA. A local combustion mode is only defined for pre-ignition mixtures ($\lambda_e > 0$), consistent with prior studies [54,55]. Furthermore, mixtures with $\lambda_e \leq 1$ are considered too slow to be reactive and are therefore ignored. The extinction mode ($\alpha < -1$) is where the ignition process is reversed by diffusion; the deflagration mode ($\alpha > 1$) is where ignition is dominantly controlled by diffusion; the auto-ignition mode ($-1 \leq \alpha \leq 1$) is where ignition is dominantly controlled by chemistry.

CEMA has been used in various flame configurations [52,56], including LTC of diesel spray simulations [57–59]. To aid in the analysis of combustion recession, a customized CEMA tool is implemented within CONVERGE 2.4 to identify the local combustion modes of the flame AEOI.

3. Results and discussions

3.1. Non-reacting spray validation

As the fuel spray evolution affects the combustion thereafter, validation of the non-reacting spray is essential to ensure accurate reacting flow predictions. The non-reacting simulations at "Spray A" conditions are analyzed to validate the spray modeling approach. The non-reacting spray conditions also include a variation of injection pressure as it is known to impact the fuel spray characteristics. As suggested by the ECN, the liquid penetration length (LPL) and vapor penetration length (VPL) are used to validate non-reacting spray conditions. The ECN definitions for LPL and VPL are adopted in this study [20]. For numerical simulations, the LPL is defined as the maximum axial penetration of 95% of the total injected fuel mass. The VPL definition is consistent for both experiments and numerical simulations and is defined as the maximum distance from the injector where the vapor fuel mass fraction is 0.1%.

Fig. 2 shows the temporal evolution of the LPL and VPL of two non-reacting cases with injection pressures of 50 MPa and 150 MPa (baseline). For clarity, it should be noted that: (i) the SOI is set up to correspond to the starting time of the simulation, i.e. 0 ms, and (ii) the non-reacting results are an ensemble average from three realizations. A quantitative comparative analysis of the liquid penetration results shows a good agreement with the experimental results for "Spray A" baseline conditions. However, there is a slight over-prediction of liquid penetration in the 50 MPa case, which could result from the reduced pressurized conditions, allowing the injected fuel to travel much faster in the time frame. On the other hand, the vapor penetration results are more varied. There is an under-prediction in the 50 MPa case which can be attributed to insufficient air entrainment (mixing), thus reducing the rate of vaporization. In contrast, a slight over-prediction in the baseline case highlights an increased rate of breakup that leads to enhanced vaporization and greater penetration into the domain. These trends are also observed in the mixture fraction space, depicted in Fig. 3. (Note: the contours that are plotted throughout this study are from a mid-plane slice at $z = 0$ mm). Regardless of the injection pressure, the spray morphologies are similar to their experimental counterparts. Overall, the discrepancy between the numerical and experimental data is less than 2% such that the results obtained can be considered sufficiently

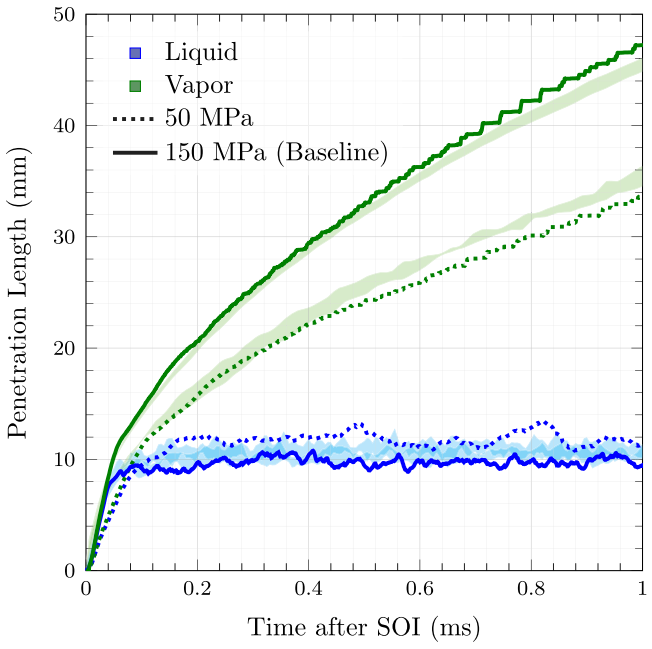

Fig. 2. Numerical liquid and vapor penetration lengths at "Spray A" conditions with injection pressures of 50 MPa and 150 MPa (baseline). The shaded areas denote experimental results. (For interpretation of the references to color in this figure legend, the reader is referred to the web version of this article.)
Source: Taken from the ECN [20].

Table 3
Ignition delay times (IDT) and flame lift-off lengths (FLOL) at "Spray A" baseline conditions for various chemical kinetic mechanisms and grid resolutions. The experimental data are obtained from the ECN [20].

	Luo (Base)	Luo (Refined)	Yao (Base)	Yao (Refined)	Experiment
IDT (ms)	0.533	0.487	0.357	0.377	0.400–0.440
FLOL (mm)	23.6	23.4	18.9	16.5	15.8–17.9

accurate.

In summary, LES of the non-reacting "Spray A" at both baseline and 50 MPa conditions provided valuable insight into the spray modeling assumptions and their implications. While the results for the baseline case agree well with the experimental data for both liquid and vapor penetrations, the 50 MPa case shows discrepancies in both the spray penetration and morphology contour plots. This implies that reduced ambient pressure conditions play a pivotal role in quantifying the degree of mixing and spray propagation. Nevertheless, the quantitative and qualitative comparisons between the numerical results and experimental data show good agreement, thus permitting further progression of the study.

3.2. Reacting spray validation

As suggested by the ECN [20], the reacting spray results can be validated by comparing their ignition delay time (IDT) and FLOL to the corresponding experimental results. For experiments, the ECN suggests IDT and FLOL to be the time and axial location where 50% of the maximum threshold of OH* chemiluminescence occurs, respectively [20]. For numerical simulations, the ECN suggests IDT to be the time where the maximum temporal change of the maximum temperature ($[dT/dt]_{max}$) occurs and FLOL to be the axial location where the hydroxyl (OH) mass fraction reaches 2% of the maximum value in the domain after the flame stabilizes, respectively [20]. In this study, the ECN standards for IDT and FLOL are adopted to validate the reacting spray simulations.

Table 3 summarizes the IDTs and FLOLs from the numerical simulations and experiments at "Spray A" baseline conditions. Both Luo and Yao mechanisms predict comparable IDTs to experimental results. However, as observed in other "Spray A" simulations [14,22,26], the Luo mechanism slightly over-predicts the IDT, whereas the Yao mechanism slightly under-predicts it. This is likely because formyl (HCO) production (R1) in the Yao mechanism is enhanced, meaning that the reaction rate is faster, relative to the detailed mechanism of the Lawrence Livermore National Library (LLNL) [60]. It should be noted that the Yao mechanism was tuned against the LLNL mechanism for IDTs [19]. Since R1 is enhanced, the production (R2) of hydroperoxyl (HO_2), a key species in tracking low-temperature ignition (LTI), becomes a dominant chemical path in the Yao mechanism [60]. Furthermore, the reaction rate of R2 is also increased (relative to the LLNL mechanism) [60]; the overall faster LTI will then lead to a faster HTI and hence a shorter IDT.

$$CH_2O + OH \rightarrow HCO + H_2O \quad (R1)$$

$$HCO + O_2 \rightarrow CO + HO_2 \quad (R2)$$

While the FLOL from the Yao mechanism agrees well with experimental measurements, the FLOL obtained with the Luo mechanism is higher than the experiment, in line with previous numerical studies [14,22,26]. The likely reason why the Luo mechanism over-predicts the IDT and FLOL is its relatively smaller chemical source term values [26], which leads to an overall slower combustion process. Nevertheless, the numerical IDT and FLOL are comparable to experimental results, which allows the authors to proceed with the analysis of the reacting spray AEOI.

3.3. Grid resolution and chemical kinetic mechanism selection

The appropriate grid resolution and chemical kinetic mechanism that "best" model and predict combustion recession are first assessed/investigated. Fig. 4 shows the OH and formaldehyde (CH_2O) mass fraction contours of the different grid resolutions and chemical mechanisms at baseline conditions. OH* chemiluminescence images from Knox et al. [17] are also plotted in Fig. 4, where the time steps (as indicated on the experimental image) correspond to after the start of ramp-down. In the context of this study, ramp-down is approximately 0.1 ms (100 μs) before EOI, therefore the time stamps between the numerical and experimental images match. CH_2O and OH are produced during LTI and HTI, respectively, and can be considered the representative species/product of the two-stage combustion process of diesel sprays. As previously mentioned, OH* is the electronically excited form of OH, and is also used to represent HTI [17].

As seen in Fig. 4, the simulation using the base grid and the Luo mechanism has no HTI upstream of the quasi-steady FLOL (denoted by red dashed lines) before EOI, indicating no combustion recession. However, while the CH_2O concentrations are decreasing with time, a small HTI kernel near the main flame does form by 0.4 ms AEOI, indicating that combustion reactions are still occurring near the FLOL. Using the same mechanism with a refined grid, combustion recession instead starts to occur at 0.3 ms AEOI, close to the main flame (the flame downstream of the FLOL). By 0.4 ms AEOI, the HTI kernels have merged with the main flame. In contrast, the simulations using the Yao mechanism at both grid resolutions show combustion recession as separate ignition kernels, which seems to be in line with other experimental studies [16,17]. With both grid resolutions, combustion recession starts to occur just before 0.2 ms AEOI. The HTI kernels start to grow in size and by 0.4 ms AEOI, they have fully developed. In addition, the simulations with both mechanisms indicate that HTI occurs near the stoichiometric mixture fraction, denoted by the solid cyan lines in Fig. 4.

When comparing the simulations to the OH* chemiluminescence imaging, simulations with the Yao mechanism seem to better predict combustion recession as HTI AEOI occurs farther upstream and as

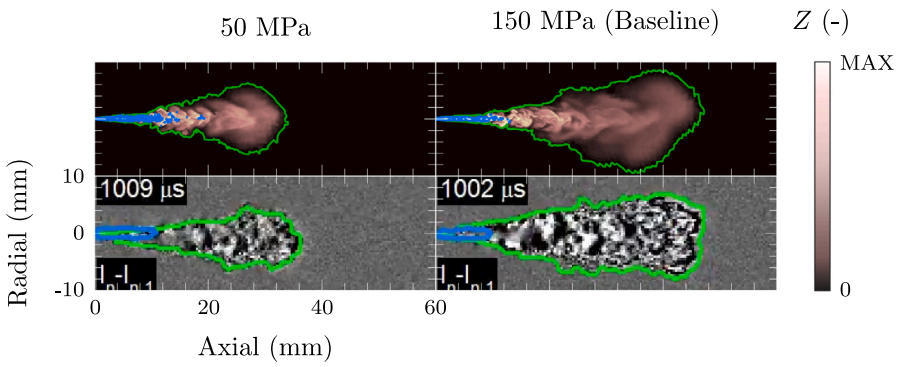

Fig. 3. Numerical spray morphology of the instantaneous mixture fraction (Z) at "Spray A" conditions (top) compared with experimental schlieren imaging (bottom) from the ECN [20] at 1 ms after SOI. The blue and green lines denote liquid and vapor boundaries, respectively. The color scale is set up to the maximum mixture fraction in the domain. (For interpretation of the references to color in this figure legend, the reader is referred to the web version of this article.)

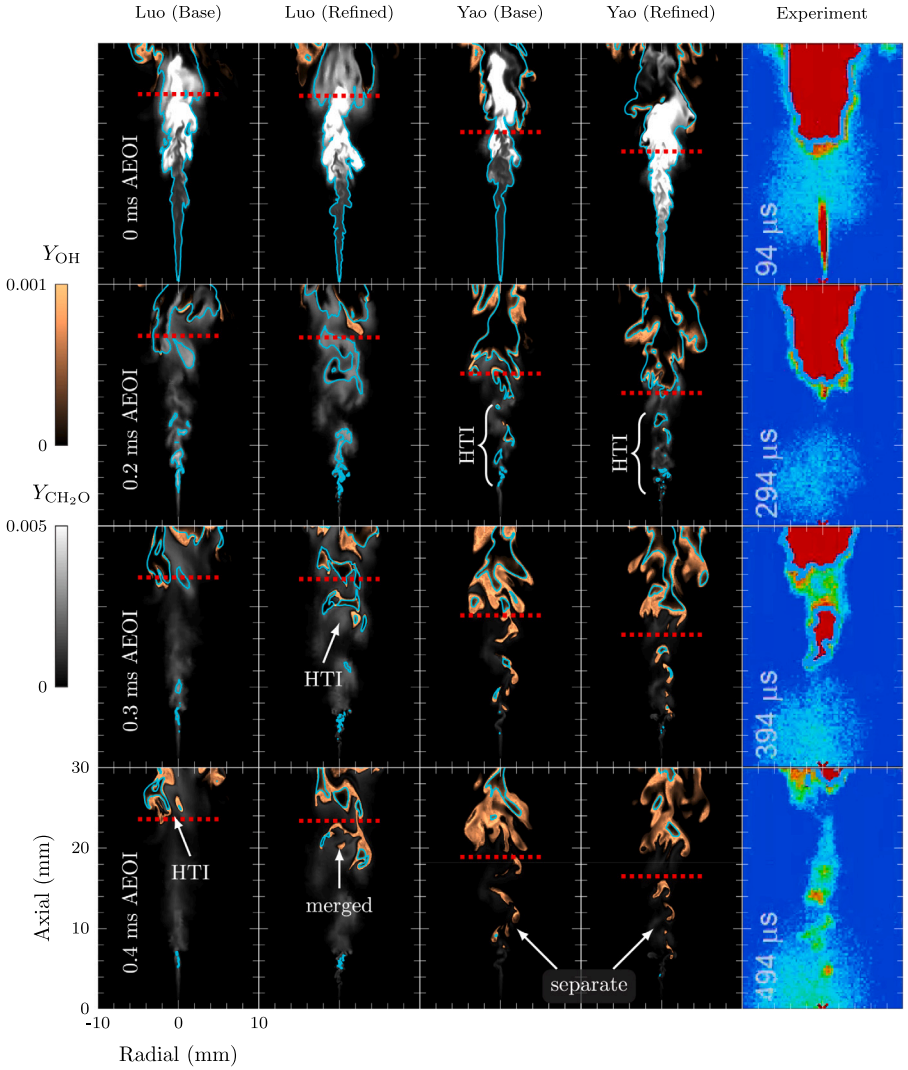

Fig. 4. OH and CH_2O mass fraction (Y) contours of different simulations compared with experimental OH* chemiluminescence imaging [17]. The experimental images are in false color scale with red set as 50% of OH* maximum intensity. The background noise in the experiments are due to soot luminosity. The experimental time steps are after the start of ramp-down; the time stamps match as EOI is approximately 0.1 ms after the start of ramp-down. The dashed red lines and the solid cyan lines indicate the quasi-steady FLOL before EOI and the stoichiometric mixture fraction isocontour, respectively. (For interpretation of the references to color in this figure legend, the reader is referred to the web version of this article.)

previously mentioned, as separate ignition kernels, which is consistent with the chemiluminescence snapshots in Fig. 4 and other experimental studies [16,17]. While combustion recession does occur in the simulations using the Luo mechanism with the refined grid, it does not exhibit the same characteristics as the chemiluminescence imaging and other experimental studies [16,17]. As mentioned previously, the chemical source term values in the Luo mechanism are relatively low, specifically in the intermediate combustion stages [26]. This likely causes the

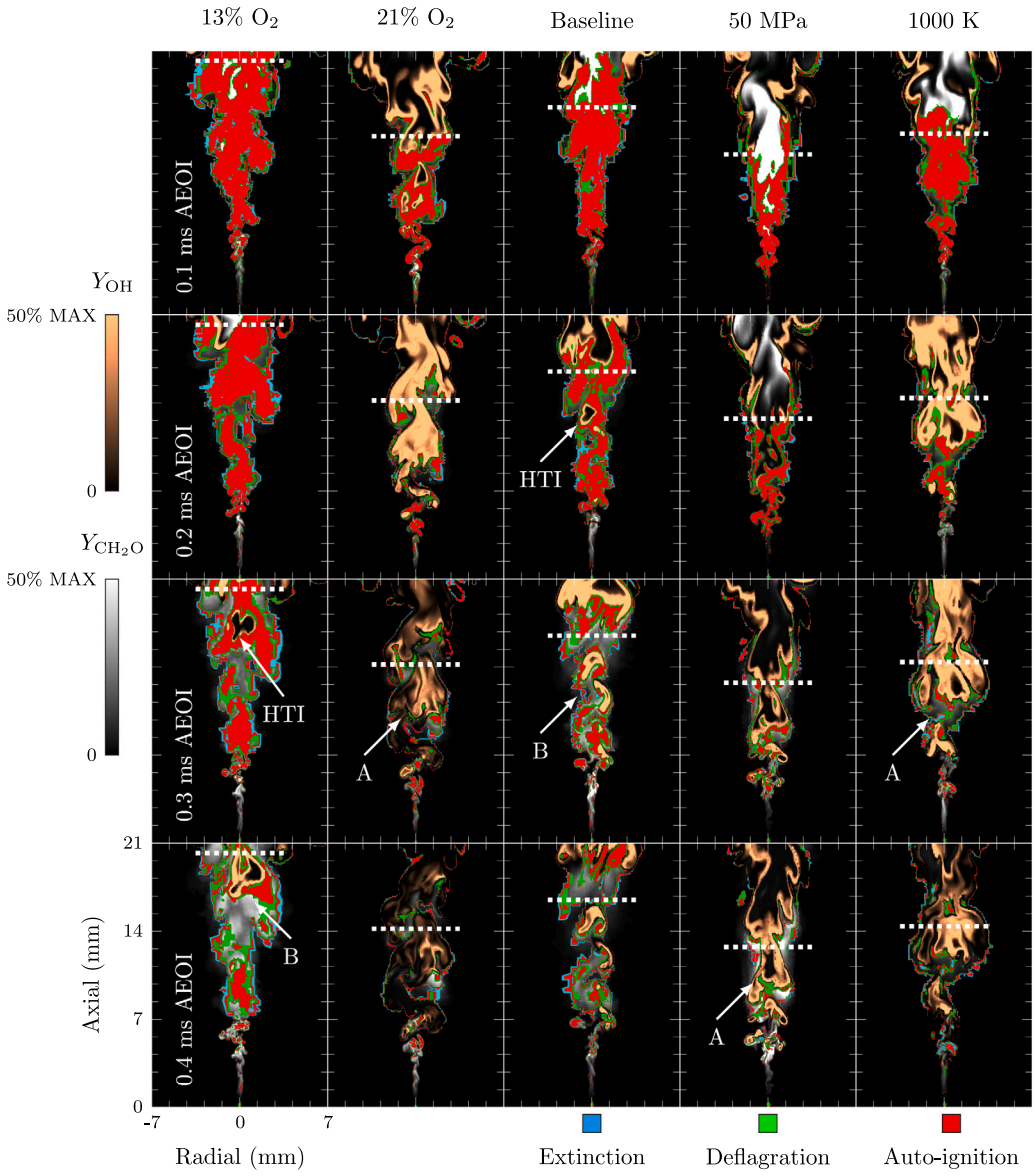

Fig. 5. Local combustion modes near the nozzle using the refined grid resolution and the Yao mechanism. The OH and CH_2O mass fraction (Y) contours are overlaid to show the combustion process, where their color scale is set up to 50% of the maximum mass fraction in the domain. The dashed white lines denote the quasi-steady FLOL. (For interpretation of the references to color in this figure legend, the reader is referred to the web version of this article.)

failure of the transition from LTI to HTI in the base grid simulation and a smaller combustion recession tail in the simulation with the refined grid for the Luo mechanism. Conversely, the simulations with both grid resolutions for the Yao mechanism predict combustion recession well. However, considering that the refined grid simulation using the Yao mechanism had slightly better reacting spray validation results, the refined grid resolution and the Yao mechanism will be considered hereafter for the analysis of local combustion modes AEOI. The authors would also like to note that a total of four realizations were performed for each chemical kinetic mechanism. However, it was determined that one realization is sufficient to characterize combustion recession. More details are provided in Appendix.

3.4. Combustion modes of combustion recession

Combustion recession is further analyzed using CEMA. The local combustion modes of the mixtures near the nozzle at different conditions are plotted in Fig. 5. The CH_2O and OH mass fractions, where their color scale is set up to 50% of their maximum value in the domain, are also plotted to show the LTI and HTI processes, respectively. In the 50 MPa, 21% O_2, and 1000 K cases, the kernels ignite and develop much more rapidly, appearing as a continuous stream that propagates towards the nozzle, denoted by "A" in Fig. 5. In contrast, the HTI kernels in the baseline and 13% O_2 cases ignite and develop relatively slower and appear as separate ignition kernels, denoted by "B" in Fig. 5. For example, the mixtures upstream of the FLOL (denoted by the dashed white lines) in both the 13% O_2 and baseline cases appear similar at 0.1 ms AEOI. However, HTI has occurred in the baseline case by 0.2 ms AEOI, whereas in the 13% O_2 case, HTI occurs around 0.3 ms AEOI.

As demonstrated in Fig. 5, the dominant mode just after EOI in all cases is auto-ignition. HTI seems to occur where the auto-ignition modes are located, supporting the previous conclusions that combustion recession is auto-ignition dominated. Interestingly, for all cases exhibiting combustion recession, the ignition kernels grow and develop in locations where the deflagration modes coincide as well. Recently, a "Spray A" study by Gong et al. [61] showed that auto-ignition induced flame fronts are HTI sites that are frequently observed in the

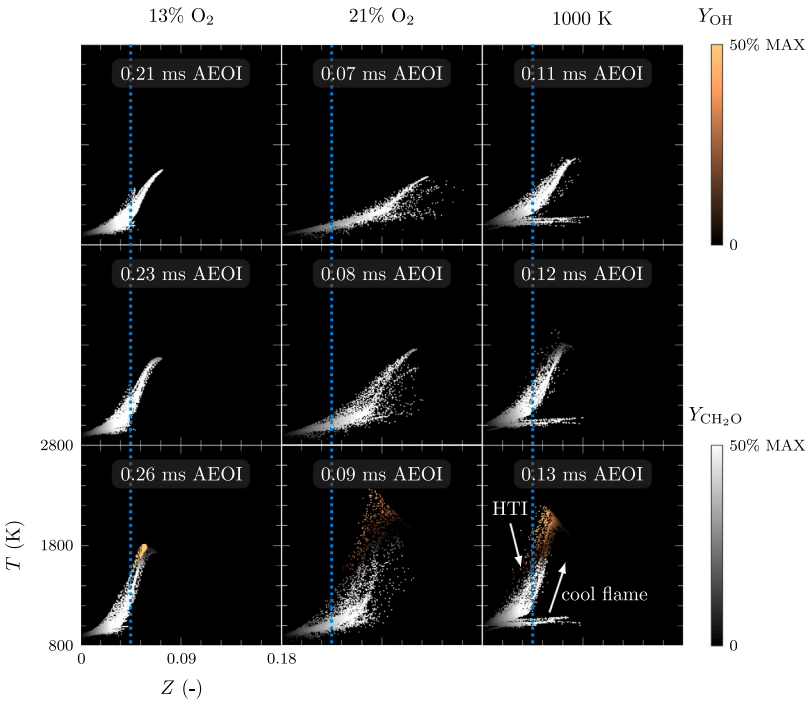

Fig. 6. CH_2O and OH mass fraction (Y) scatter plot in temperature–mixture fraction (T–Z) space of the 13% O_2, 21% O_2, and 1000 K cases. Only the domain area upstream the quasi-steady FLOL are plotted. The dashed cyan lines denote stoichiometric mixture fraction. The color scale is set up to 50% of the maximum mass fraction in the domain. (For interpretation of the references to color in this figure legend, the reader is referred to the web version of this article.)

rich core of mixtures [61]. Furthermore, they found that these auto-ignition induced flame fronts are stabilized by flame propagation. This can perhaps explain why the ignition kernels AEOI (or combustion recession) grow and develop as deflagration. Similar results have been found in closely resembling "Spray A" DNS studies performed by Farjam et al. [62] and Zhou et al. [63], where they found that HTI transitions into a deflagration after auto-ignition. Although not visible in Fig. 5, the authors have observed that deflagration modes exist in the center of the ignition kernels just before HTI. While the results support previous experimental studies where combustion recession was auto-ignition dominated, the presence of a deflagration mode within the kernel just before HTI warrants further investigation.

3.4.1. *Re-ignition mechanism*

To further analyze combustion recession, the first HTI kernels upstream of the quasi-steady FLOL AEOI in the 13% O_2, 21% O_2, and 1000 K cases are temporally located; the time steps just before the ignition of these kernels are also considered. Fig. 6 shows the CH_2O and OH mass fractions upstream of the FLOL in T–Z space. The stoichiometric mixture fraction is denoted by the dashed cyan lines. Similar to Fig. 5, the color scale is set up to 50% of the maximum mass fraction in the domain for visibility.

As depicted in the bottom three plots of Fig. 6, combustion recession, indicated by OH, first occurs at 0.26 ms AEOI for the 13% O_2 case, 0.09 ms AEOI for the 21% O_2 case, and 0.13 ms AEOI for the 1000 K case. The lower oxygen concentration results in a relatively delayed combustion recession due to decreased reactivity, occurring about 0.15 ms later compared to the high reactivity cases. Conversely, because of their increased reactivity, HTI occurs earlier in the 21% O_2 and 1000 K cases. Specifically for the 1000 K case, HTI seems to also occur around the stoichiometric mixture fraction. This has also been observed in the aforementioned "Spray A" DNS study by Zhou et al. [63]. In their study, they found that a cool flame with LTI products propagates towards the rich core while at higher ambient temperatures, HTI can also occur in relatively leaner areas outside the rich region [63]. These observations are seen in Fig. 6 where OH concentrations are much higher near the cool flame, denoted by CH_2O.

The cool flame phenomenon in *n*-dodecane sprays has been studied by Zhong et al. [58], where they found that a cool flame propagates towards fuel-rich regions, mixing in the LTI products and increasing the temperatures, thereby promoting HTI. In the same "Spray A" DNS studies [62,63] mentioned previously, the authors observed that in lower reactivity mixtures, the cool flame deflagrates towards the rich core region. This is likely the reason why a deflagration mode exists within the kernel as the cool flame propagates into the rich mixtures, promoting mixing and increasing the overall projected diffusion source terms to the CEM. This perhaps relates to the fundamental basis of species diffusion where one can suppose that the local temperature increase, induced by the cool flame, favors species to diffuse faster into the surroundings, and igniting the mixture as either a continuous stream of ignition or separate ignition kernels (depending on the ambient thermodynamic conditions). Nevertheless, some additional in-depth research on this topic is required to strengthen the claims made here. It should be noted, while deflagration is essential in assisting the full development of the combustion recession, auto-ignition is still found to dominate the combustion recession process as the deflagration mode constitutes only a small part of the HTI kernel before ignition.

To further characterize the deflagration processes in combustion recession and the impact of mixture stratification, the probability density functions of the mixture fraction of the mixtures upstream of the FLOL AEOI in the three aforementioned cases are plotted in Fig. 7. The mixture fraction is conditioned based on either the deflagration or auto-ignition mode. Similar to the previous discussion, the time step for each case is when the first HTI upstream of the FLOL AEOI occurs. As seen in the 1000 K case, auto-ignition modes are slightly more concentrated on the leaner regions, consistent with previous findings that auto-ignition can occur in leaner regions at higher ambient temperatures [63]. Specifically for the 13% O_2 case, the likely reason why the auto-ignition modes are wholly concentrated in leaner regions is the instantaneous HTI in the mixture, thereby "consuming" the auto-ignition modes in the richer regions. Across all three cases, two mixture fraction values, one lean and one rich, occur the most frequently for the deflagration

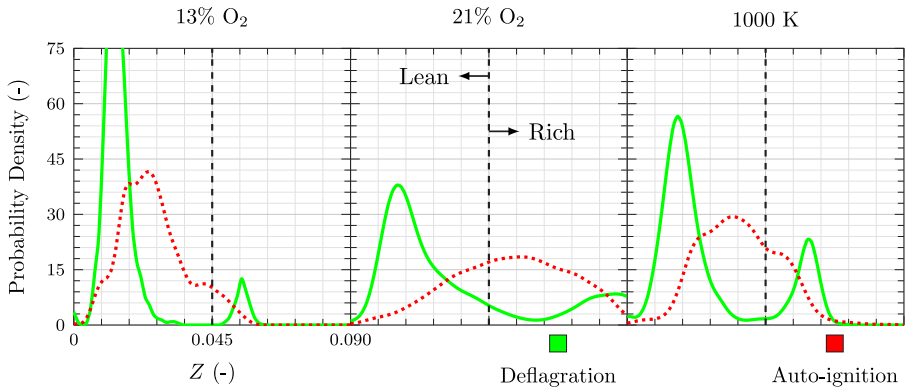

Fig. 7. The probability density functions of the mixture fraction (Z) for the 13% O_2, 21% O_2, and 1000 K cases. The mixture fraction is conditioned based on the deflagration and auto-ignition modes from CEMA. Only the area upstream the quasi-steady FLOL are considered and the time step is when HTI first occurs in each respective case.

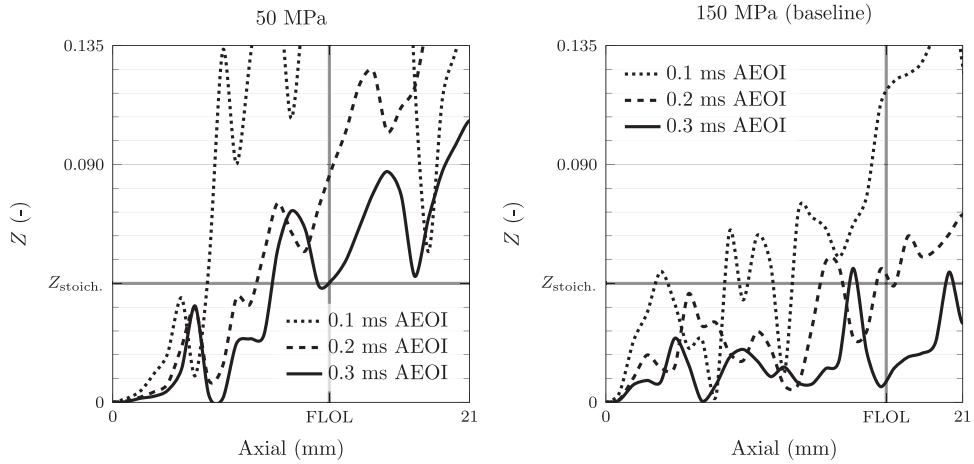

Fig. 8. Time evolution of the mixture fraction (Z) along the spray center line of the 50 MPa (left) and the 150 MPa/baseline (right) cases.

modes, as indicated by the density peaks. Although not shown, it was determined that: (i) the lean deflagration modes are associated with the propagation of the flame AEOI, and (ii) the rich deflagration modes are associated with the cool flame propagation. As discussed previously, the cool flame propagates into the fuel-rich mixtures, explaining the deflagration modes in the rich mixtures. The deflagrative waves after auto-ignition were observed to propagate to lean and stoichiometric mixtures in previous diesel surrogate studies [61,64–66]. In particular, a diesel surrogate DNS study by Krisman et al. [65] found that the auto-ignited flame propagates and expands into the leaner mixtures. This propagation enables the stoichiometric mixtures to auto-ignite [65], explaining the absence of deflagration modes (and the presence of auto-ignition modes) around the stoichiometric mixture fraction, as observed in Fig. 7. This observation highlights not only the LTI deflagrative waves but also the HTI expansion that further promotes auto-ignition. As the cool flame products are eventually consumed in the HTI process, the lean deflagrative wave will be the dominant deflagration mode in combustion recession.

The previous discussion mentioned that combustion recession is affected by the reactivity of the mixture through the increase in ambient temperatures and/or oxygen concentrations. Although the 50 MPa case would have the same ambient temperature and oxygen concentration as the 150 MPa (baseline) case, as seen in Fig. 5, combustion recession is more prevalent in the 50 MPa case. To further elucidate this, Fig. 8 shows the temporal evolution of the mixture fraction along the spray center line for the 50 and 150 MPa (baseline) cases. In both cases, the mixture fraction decreases because of the mixing due to the entrainment wave. However, in the 50 MPa case, the mixtures stay relatively richer as time advances, which allows them to undergo HTI. As previously mentioned, Zhang et al. [34] observed that higher injection pressures result in larger entrainment waves AEOI. In the same study, they also observed that lower injection pressures result in a reduced axial velocity at EOI [34]; a reduced axial velocity at EOI reduces the overall entrainment rate. Since the entrainment near the upstream mixtures is weaker, the mixtures remain the near-stoichiometric mixture fraction (approximately 0.045) relatively longer, which allows HTI, or combustion recession, to occur [34].

To demonstrate the general trend of the local combustion modes upstream of the FLOL AEOI, the temporal evolution of the fraction of these modes is plotted in Fig. 9. The 800 K case is excluded as it does not exhibit combustion recession, as discussed in the next section. In all cases, the auto-ignition modes form the majority of the local combustion modes AEOI. As time progresses, the deflagration modes start to increase, indicating the transition of the HTI kernels from an auto-ignition mode to a deflagrative wave, which was observed in the previous discussions. However, all cases seem to reach an equilibrium between the decreasing auto-ignition and the increasing deflagration modes at around 0.4 ms AEOI; all cases also show the extinction modes gradually increasing. These observations suggest that, regardless of initial conditions, combustion recession is most likely a process that is initially auto-ignitive, and then propagation-driven until reaching a diffusive limit where, as discussed in the next section, the diffusion processes render the upstream flame extinct.

3.4.2. *Extinction mechanism*

Perhaps more interestingly, no combustion recession occurs with an ambient temperature of 800 K, consistent with previous studies [14,17].

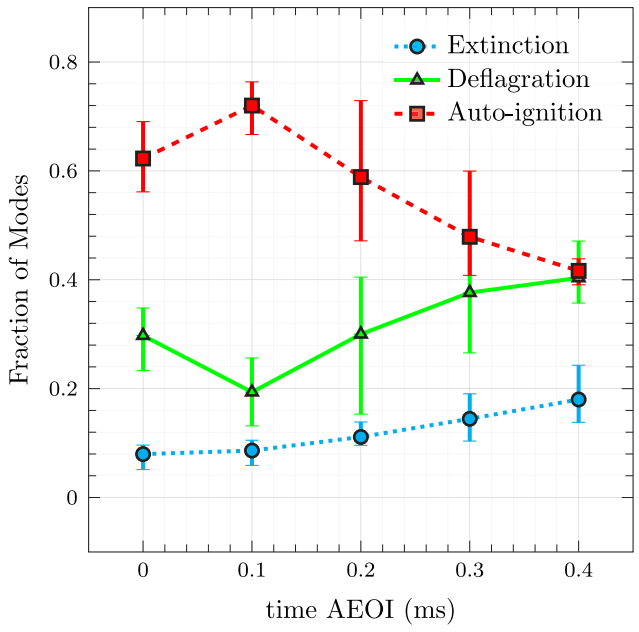

Fig. 9. The temporal evolution of the mean fraction of local combustion modes across all cases except the 800 K case. The lower and upper ranges denote the minimum and maximum fraction across the cases, respectively.

In order to study this in detail, Fig. 10 shows the local combustion modes AEOI, entrainment, and mixture fraction evolution of the 800 K case. The middle and right-most contours of Fig. 10A illustrate that the auto-ignition modes start to transition into deflagration at around 0.2 ms AEOI. Between 0.2 and 0.3 ms AEOI, the deflagration modes then start to transition into extinction modes. By 0.4 ms AEOI, the area between the FLOL and the injector nozzle is dominated by extinction, fully suppressing the combustion process.

In the left-most contours of Fig. 10A, a relatively large entrainment wave, due to a longer FLOL (20.5 mm as opposed to 16.5 mm in the baseline case), is present near the injector nozzle AEOI. In addition, entrainment recirculation (encircled in red in Fig. 10A) is present close to the upstream mixtures. To complement these findings, the temporal evolution of mixture fraction along the spray center line at the same condition is plotted in Fig. 10B. Rich pockets in the near-nozzle region exist at 0.2 ms AEOI. However, due to the entrainment wave and recirculation along this region, the mixtures become leaner. By 0.4 ms AEOI, the region has become fully lean. As the reactants over-mix due to the entrainment wave, the mixture becomes too lean to support HTI [9], which can potentially explain the transition from the deflagration modes to the extinction modes.

To quantifiably visualize extinction AEOI, the normalized projected chemical ($\phi_{\omega,\text{norm.}}$) and diffusion ($\phi_{s,\text{norm.}}$) source terms along the spray center at two different time steps are plotted in Fig. 10C and D. These projected source term values are normalized using the largest magnitude of either ϕ. According to Eq. (7) and the criteria for local combustion modes, extinction occurs when ϕ_s is negative, and its absolute value exceeds ϕ_ω. It should be noted that ϕ_ω is chosen to be always positive as chemistry always contributes positively to the ignition process. Fig. 10C shows that immediately after EOI, ϕ_ω dominates near-nozzle mixtures, with minimal contribution from ϕ_s. However, well after EOI (Fig. 10D), ϕ_ω significantly decreases and ϕ_s becomes predominantly negative, indicating that diffusion is inhibiting the ignition process. These observations highlight that the diffusion processes in extinction modes negatively impact the flame, leading to its suppression.

3.4.3. *Effects of scalar dissipation rate on re-ignition and extinction*

As proposed by literature, the scalar dissipation rate represents the rate of mixing of scalar values, which makes it essential in determining the effects of turbulence on combustion [67]. Studies have suggested that HTI and extinction occur at low and high scalar dissipation rates, respectively [68]. Therefore, to study the effects of scalar dissipation rate on combustion recession, Fig. 11 shows the OH and CH_2O mass fractions (the color scale is set up to 50% of the maximum mass fraction in the domain) and scalar dissipation rates at the time and location where HTI occurs AEOI in baseline and 800 K conditions.

Encircled in red and white are the spatial locations of the HTI kernels AEOI for the baseline and 800 K cases. It should be noted that the HTI kernel in the 800 K case is located at the very base of the main flame, and is therefore not considered to be combustion recession in this case. As expected, both kernels occur near stoichiometric mixture fraction, denoted by the cyan lines. They also appear in areas with low scalar dissipation, occurring at $\chi \approx 1\ s^{-1}$. In fact, although not shown for brevity, the scalar dissipation rates in the upstream mixtures AEOI in all cases are low ($\chi <\sim 1\ s^{-1}$). This indicates that, as expected, low scalar dissipation rates allow the species and temperature to accumulate, promoting HTI [68]. The 800 K case also exhibits low scalar dissipation rates AEOI. However, the flame in the 800 K case extinguishes without combustion recession. As previously mentioned, the lower reactivity found in lower ambient temperatures is not favorable for HTI. In addition, the cool flame and the entrainment AEOI lean the mixtures upstream of the FLOL, further inhibiting combustion. While low scalar dissipation rates support the auto-ignition process AEOI, this process is also dependent on other factors affecting the overall reactivity of the mixture, including ambient conditions and fuel mixing AEOI.

3.5. *Combustion recession metrics*

Finally, metrics are presented to generalize combustion recession. First introduced by Knox et al. [15], the combustion recession metric, R, represents the fraction of ignited mixtures upstream of the FLOL AEOI. Through variations of the "Spray A" conditions, the ensemble average of the combustion recession metric, $\langle R \rangle$, was obtained [15]. A standard least squares regression on the ensemble average of the metric was then performed, resulting in the equation:

$$\begin{aligned}\langle R \rangle = &-0.3618 - 0.1686\rho + 3.014\times10^{-4}T + 0.4576O_2 + 6.372\times10^{-4}d_0 \\ &+ 1.998\times\rho T \begin{cases} -0.0437 & \text{if ramp-down is fast} \\ +0.0437 & \text{if ramp-down is slow} \end{cases} \\ &+ 0.1054\rho O_2 + 8.772\times10^{-5}\rho d_0 - 1.228\times10^{-4}P_{\text{inj}},\end{aligned} \tag{8}$$

where ρ, T, O_2, d_0, and P_{inj} are ambient density (kg/m^3), ambient temperature (K), oxygen concentration (%), nozzle diameter (μm), and injection pressure (bar), respectively. In the same study [15], the authors identified 3 types of combustion recession: (i) **complete combustion recession** characterized by relatively shorter mixing time scales where combustion recession occurs in lean mixtures as a continuous stream of HTI, (ii) **partial combustion recession** where the mixing time scales are even shorter and combustion recession occurs as separate HTI kernels, and (iii) **no combustion recession** where no HTI upstream of the FLOL AEOI takes place [15].

The ensemble average of the combustion recession metric has shown to be successful in determining the type of combustion recession in a wide range of test conditions [15]. In fact, as shown later, the metric correctly predicts the type of combustion recession in the numerical results of this study. However, it only predicts the type of combustion recession from the test conditions and does not quantify how much of the upstream mixtures have ignited. Therefore, to complement this metric, the authors propose a new criterion for combustion recession,

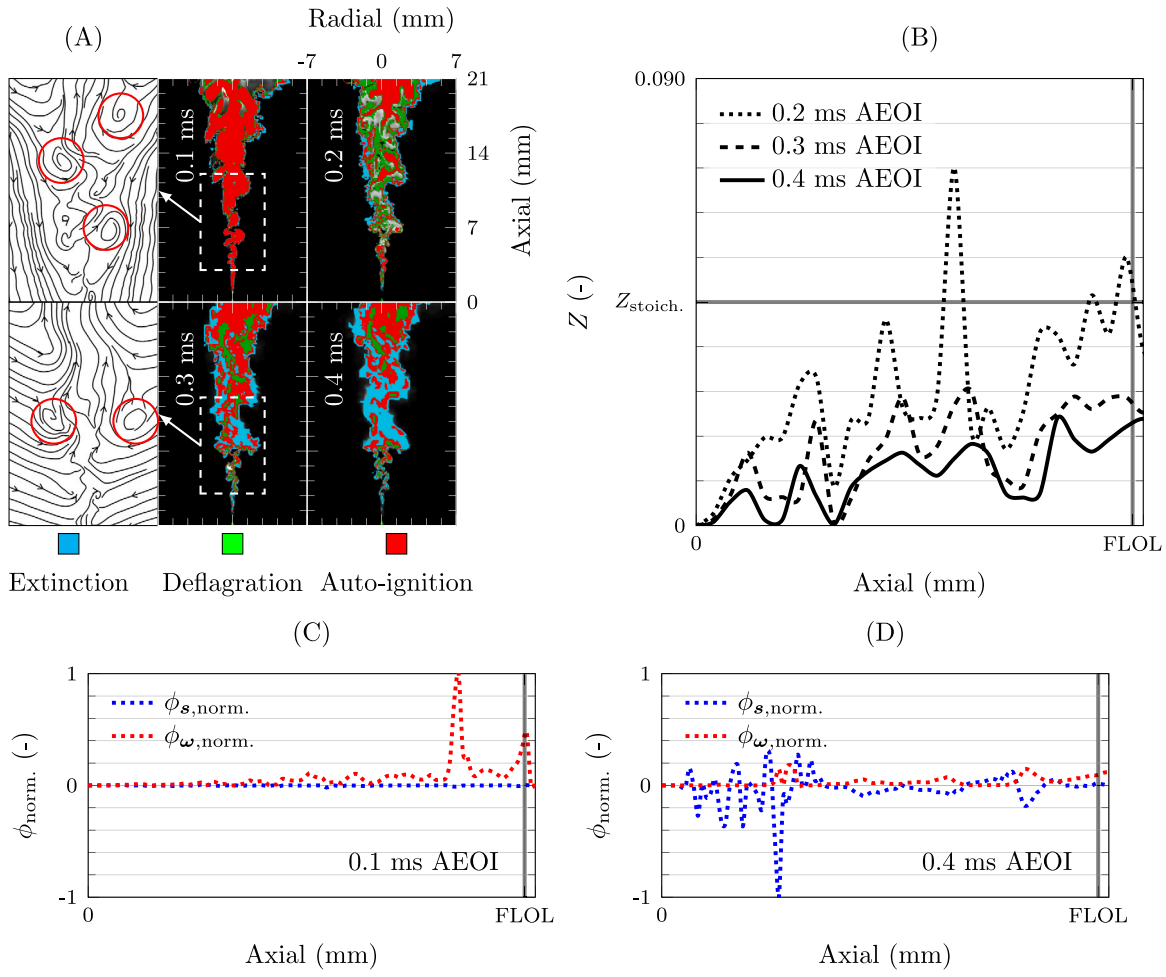

Fig. 10. (A) Local combustion modes of the 800 K case determined by CEMA. The OH and CH_2O mass fraction contours are overlayed to show the combustion process. The plots on the left show a close-up of the velocity streamlines. The red circles denote entrainment recirculation. (B) Time evolution of the mixture fraction (Z) along the spray center line of the 800 K case. The normalized projected chemical ($\phi_{\omega,\text{norm.}}$) and diffusion ($\phi_{s,\text{norm.}}$) source terms along the spray center line at (C) 0.1 ms AEOI and (D) 0.4 ms AEOI. (For interpretation of the references to color in this figure legend, the reader is referred to the web version of this article.)

R_{λ_e}, based on λ_e within the CEMA framework:

$$R_{\lambda_e} = \frac{\Omega_{\text{non-explosive}}}{\Omega_{\text{non-explosive}} + \Omega_{\text{explosive}}}, \tag{9}$$

where $\Omega_{\text{non-explosive}}$ and $\Omega_{\text{explosive}}$ represent the regions of non-explosive (ignited) and explosive (pre-ignition) mixtures upstream of the FLOL, respectively. As previously mentioned, explosive mixtures are characterized by $\lambda_e > 0$. Conversely, non-explosive mixtures are characterized by $\lambda_e < 0$. To extend these definitions, values of $|\lambda_e| < 1$ are truncated as the chemical Jacobian near the λ_e zero-crossing becomes defective [51]. The formulation of R_{λ_e} is similar to R which, as previously stated, also measure the fraction of ignited mixtures. However, R relies on line-of-sight measurements, consequently only considering the upstream mixtures in the axial dimension. Since R_{λ_e} numerically considers the mixtures in multi-dimensional space, i.e. the axial dimension and the radial dimension, it can represent more accurately the fraction of the mixtures that have undergone HTI.

Fig. 12 shows $\langle R \rangle$ for each boundary condition and R_{λ_e} of the numerical results in this study. From $\langle R \rangle$, it is illustrated that only the 800 K case is predicted to have **no combustion recession**. The higher reactivity conditions, 21% O_2 and 1000 K, are predicted to have **complete combustion recession**, and the baseline and 13% O_2 cases are indicated to have **partial combustion recession**. As injection pressure lowers, combustion recession becomes **complete combustion recession**. In terms of the proposed criterion, an R_{λ_e} value of 0 indicates no mixtures undergo HTI, and an R_{λ_e} value of 1 indicates all mixtures undergo HTI. For instance, for the 800 K case, R_{λ_e} indicates that almost none of the upstream mixtures sustain HTI, which is observed through the lack of OH AEOI in Fig. 5. For the 21% O_2 case, R_{λ_e} indicates a majority (approximately 80%), but not all of the upstream mixtures undergo HTI, as indicated by the presence of CEMs and CH_2O well after EOI, as also seen in Fig. 5.

Interestingly, if one assumes that R_{λ_e} uses the same criteria for the type of combustion recession as $\langle R \rangle$, then R_{λ_e} "predicts" the same type of combustion recession as $\langle R \rangle$ in all test conditions in this study except for the 50 MPa case. Indeed, R_{λ_e} "predicts" partial combustion recession instead of complete combustion recession (from $\langle R \rangle$ and the results in this study). A likely reason is that injection pressures do not relatively affect combustion recession when compared to other parameters, such as ambient temperatures [15]. Another possible reason is that the time step for calculating R_{λ_e} is chosen where all cases appear to have completed reacting, similar to the approach for the original metric [15]. However, it is noteworthy that R_{λ_e} for the 50 MPa case is near the threshold between partial and complete combustion recession. Despite this minor discrepancy between results, R_{λ_e} can accurately represent the fraction of mixtures that have undergone HTI, thereby making it an effective metric in quantifying combustion recession. Furthermore, the authors would like to highlight that the proposed metric can be a valuable computational diagnostics tool especially when the high-fidelity simulation data becomes excessive for the study of combustion recession. The identification of combustion recession can be achieved through this simple post-processing quantity which otherwise might

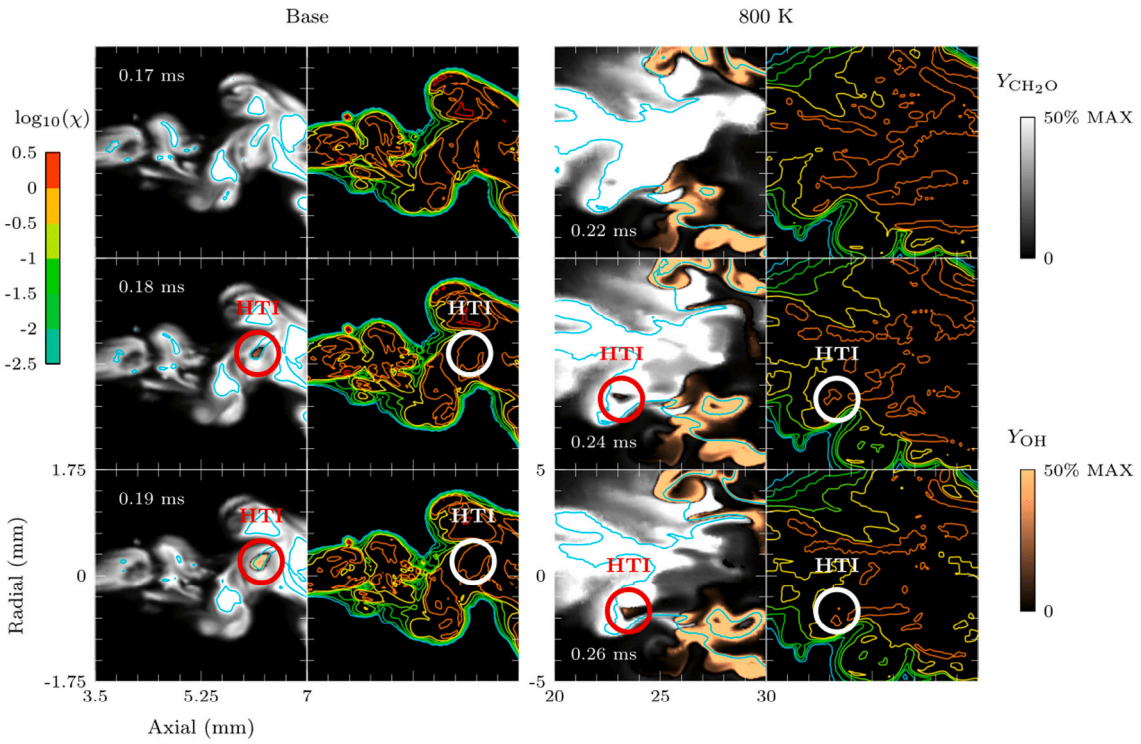

Fig. 11. Mass fraction (Y) and scalar dissipation rate (χ) contours of the baseline case (left) and the 800 K case (right). The time steps are AEOI. The cyan lines denote the stoichiometric mixture fraction. HTI is encircled in red. The color scale for the mass fractions is set up to 50% of the maximum mass fraction in the domain. (For interpretation of the references to color in this figure legend, the reader is referred to the web version of this article.)

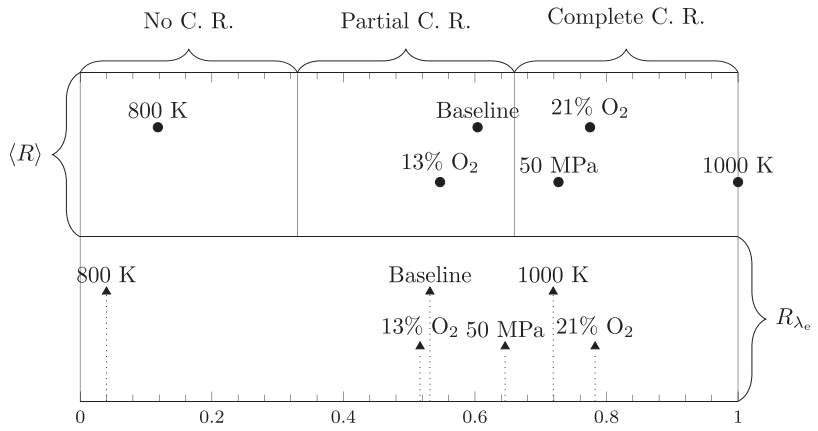

Fig. 12. The ensemble average of the combustion recession metric ($\langle R \rangle$) and the modified combustion recession metric (R_{λ_e}) for each boundary condition. For R_{λ_e}: (i) a value of 0 indicates none of the mixtures upstream of the FLOL AEOI have undergone HTI, and (ii) a value of 1 indicates all of the mixtures upstream of the FLOL AEOI have undergone HTI.

take a very long time for conventional contour plot analysis.

4. Conclusion

In this study, an *n*-dodecane spray flame at low-temperature combustion conditions was simulated with high-fidelity LES to understand the mechanism of combustion recession. A customized Chemical Explosive Mode Analysis (CEMA) tool was implemented in the CONVERGE CFD solver to determine the local combustion modes of the reacting spray after end-of-injection (AEOI). The numerical simulations at "Spray A" baseline conditions were able to accurately capture the combustion recession characteristics. The simulations using the refined grid resolution and the Yao mechanism predicted flame characteristics and combustion recession slightly better than the base grid resolution and were used to analyze the local combustion modes AEOI. For all boundary conditions tested in this study, except in the 800 K ambient temperature case, combustion recession occurs as either a continuous stream of ignition or separate ignition kernels.

Furthermore, it was confirmed that combustion recession is auto-ignition dominated. However, deflagration modes were found to exist around the periphery of the ignition kernels, indicating that after auto-ignition, combustion recession propagates as deflagration. At higher ambient temperatures, auto-ignition induced flame fronts, which in the context of this study can be considered to be the high-temperature ignition (HTI) kernels AEOI, are both stabilized by and transition into deflagration; this is most likely the reason why the periphery of the ignition kernels coincides with the deflagration modes. The deflagrative wave then propagates into the leaner mixtures, which allows the stoichiometric mixtures to auto-ignite. Additionally, deflagration modes exist in the center of the kernel just before HTI. This is because a cool

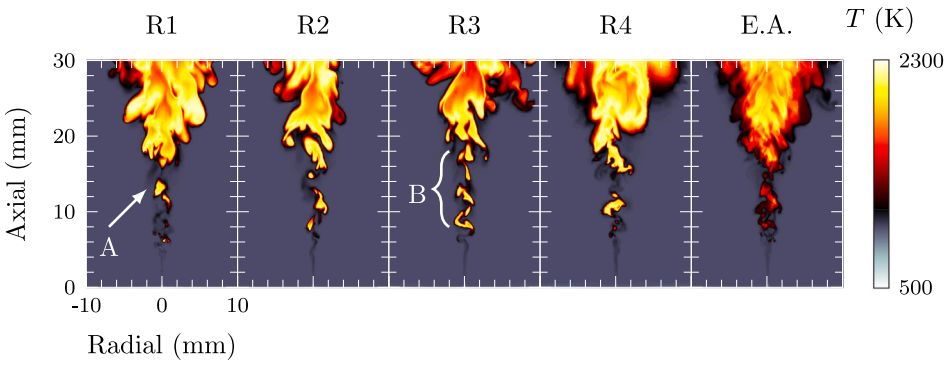

Fig. A.13. Temperature (T) contours from different realizations at "Spray A" baseline conditions using the Yao mechanism (E.A. stands for Ensemble Average). The time step is 0.2 ms AEOI.

flame propagates towards the inner fuel-rich regions, promoting mixing and increasing the temperatures, which promotes HTI.

Moreover, combustion recession occurs further upstream with a lower injection pressure as the reduction in axial velocity decreases the entrainment magnitude. The mixtures near the nozzle stay near the stoichiometric mixture fraction longer due to weaker entrainment, supporting HTI. Conversely, the entrainment wave in lower reactivity mixtures overleans the mixture, rendering it unable to support HTI, which leads to the extinction of the upstream flame AEOI. In addition, combustion recession was found to occur in areas with low scalar dissipation rates. However, due to the previous results, combustion recession also seems to be dependent on the chemical and diffusion processes. Finally, a new criterion for combustion recession is proposed to take into account combustion recession in multi-dimensional space complementing the original metrics developed through experiments. The new criterion is formulated to represent the fraction of HTI in mixtures upstream of the flame lift-off length AEOI. All numerical results match the combustion recession characteristics predicted by both previous and proposed metrics, supporting the findings of this study.

CRediT authorship contribution statement

F.J. Arguelles: Writing – review & editing, Writing – original draft, Visualization, Methodology, Investigation, Formal analysis, Data curation, Conceptualization. **M.D. Fagade:** Writing – original draft, Visualization, Validation, Investigation, Formal analysis, Data curation. **J. Mehra:** Writing – review & editing, Visualization, Data curation, Conceptualization. **C. Xu:** Writing – review & editing, Methodology, Conceptualization. **N. Sekularac:** Writing – review & editing, Visualization, Supervision, Methodology, Investigation, Conceptualization. **X.H. Fang:** Writing – review & editing, Writing – original draft, Supervision, Project administration, Investigation, Funding acquisition, Data curation, Conceptualization.

Declaration of competing interest

The authors declare that they have no known competing financial interests or personal relationships that could have appeared to influence the work reported in this paper.

Acknowledgments

The authors gratefully acknowledge the Natural Sciences and Engineering Research Council of Canada and Alberta Innovates for their financial support. The authors also thank the Research Computing Services group at the University of Calgary for supporting all simulations conducted in this study and Convergent Science for their CONVERGE CFD Software and financial support. The work at Argonne National Laboratory was supported by the U.S. Department of Energy, Office of Energy Efficiency and Renewable Energy, under contract DE-AC02-06CH11357. We appreciate the review and comments from Dr. Schuyler Hinman for the Computational Setup section and the help from Peter Siemens on visualizing the figures.

Appendix. Realization variations

As previously mentioned, simulations with the refined grid resolution and the Yao mechanism will be used to study combustion recession. However, the realization-to-realization variations in LES can affect the subsequent analysis of the system. In a "Spray A" study by Pei et al. [47], it was found that five LES realizations are required to obtain 99% similarity to an equivalent of 16 LES simulations for mixture fraction [47]. However, the study also determined that more realizations are needed depending on the scalar of interest [47]. A similar spray study by Bao et al. [69] found analogous results that scalar variables with larger scale fluctuations require more realizations. However, Fang [37] has accurately predicted the reacting "Spray A" characteristics before EOI with only five realizations. Furthermore, an LES of "Spray A" split-injections by Blomberg et al. [70] predicted combustion recession, also with five realizations. Each of their realizations predicted combustion recession, albeit in different spatial locations.

To illustrate the realization-to-realization variation of combustion recession in this study, the temperature contours at "Spray A" baseline conditions of each realization and their ensemble average using the Yao mechanism are presented in Fig. A.13. As seen in the figure, each realization exhibits different spatial characteristics of combustion recession. For example, combustion recession in R1 is indicated by one largely developed HTI kernel, denoted by "A", with smaller kernels near the nozzle. In contrast, combustion recession in R3 is marked by multiple developed HTI kernels, denoted by "B". Nevertheless, combustion recession occurs as separate HTI kernels in all four realizations, consistent with previous experimental results [16]. As expected, the ensemble average shows much lower upstream temperatures due to the difference in the spatial locations of HTI. The results show that combustion recession, which is highly fluctuating and unsteady by nature, is affected by perturbations in the mixture, changing the spatial characteristics of the HTI kernel. However, these perturbations do not seem to affect the prediction of the combustion recession event itself. This implies that the underlying physics associated with HTI upstream of the FLOL AEOI remains the same. Therefore, one can suppose that one realization is sufficient for combustion recession analysis, as long as the combustion event itself is predicted. Hence, we use one realization (per parametric case) to study the HTI upstream of the FLOL AEOI.

References

[1] T. Pachiannan, W. Zhong, S. Rajkumar, Z. He, X. Leng, Q. Wang, A literature review of fuel effects on performance and emission characteristics of low-temperature combustion strategies, Appl. Energy 251 (2019) 113380.

[2] R. Hasegawa, H. Yanagihara, HCCI combustion in DI diesel engine, SAE Trans. (2003) 1070–1077.

[3] K. Okude, K. Mori, S. Shiino, T. Moriya, Premixed compression ignition (PCI) combustion for simultaneous reduction of NOx and soot in diesel engine, SAE Trans. (2004) 1002–1013.

[4] K. Inagaki, T. Fuyuto, K. Nishikawa, K. Nakakita, I. Sakata, Dual-Fuel PCI Combustion Controlled by In-Cylinder Stratification of Ignitability, Tech. rep., SAE Technical Paper, 2006.

[5] M. Wissink, R.D. Reitz, Direct dual fuel stratification, a path to combine the benefits of RCCI and PPC, SAE Int. J. Engines 8 (2015) 878–889.

[6] T. Nishimura, K. Satoh, S. Takahashi, K. Yokota, Effects of fuel injection rate on combustion and emission in a DI diesel engine, SAE Trans. (1998) 1894–1900.

[7] T. Lachaux, M.P. Musculus, In-cylinder unburned hydrocarbon visualization during low-temperature compression-ignition engine combustion using formaldehyde PLIF, Proc. Combust. Inst. 31 (2007) 2921–2929.

[8] B.R. Petersen, I.W. Ekoto, P.C. Miles, An investigation into the effects of fuel properties and engine load on UHC and CO emissions from a light-duty optical diesel engine operating in a partially premixed combustion regime, SAE Int. J. Engines 3 (2010) 38–55.

[9] M.P. Musculus, T. Lachaux, L.M. Pickett, C.A. Idicheria, End-Of-Injection Over-Mixing and Unburned Hydrocarbon Emissions in Low-Temperature-Combustion Diesel Engines, Tech. rep., SAE Technical Paper, 2007.

[10] S. Kook, L.M. Pickett, M.P. Musculus, Influence of diesel injection parameters on end-of-injection liquid length recession, SAE Int. J. Engines 2 (2009) 1194–1210.

[11] N. Maes, M. Meijer, N. Dam, B. Somers, H.B. Toda, G. Bruneaux, S.A. Skeen, L.M. Pickett, J. Manin, Characterization of Spray A flame structure for parametric variations in ECN constant-volume vessels using chemiluminescence and laser-induced fluorescence, Combust. Flame 174 (2016) 138–151.

[12] M.P. Musculus, K. Kattke, Entrainment waves in diesel jets, SAE Int. J. Engines 2 (2009) 1170–1193.

[13] B. Knox, C. Genzale, Effects of end-of-injection transients on combustion recession in diesel sprays, SAE Int. J. Engines 9 (2016) 932–949.

[14] D. Jarrahbashi, S. Kim, C.L. Genzale, Simulation of combustion recession after end-of-injection at diesel engine conditions, J. Eng. Gas Turbines Power 139 (2017) 102804.

[15] B.W. Knox, C.L. Genzale, Scaling combustion recession after end of injection in diesel sprays, Combust. Flame 177 (2017) 24–36.

[16] C. Koci, G.C. Martin, T. Bazyn, W. Morrison, K.I. Svensson, C.R. Gehrke, The influence of diesel end-of-injection rate shape on combustion recession, SAE Int. J. Engines 8 (2015) 647–659.

[17] B.W. Knox, C.L. Genzale, L.M. Pickett, J.M. Garcia-Oliver, W. Vera-Tudela, Combustion recession after end of injection in diesel sprays, SAE Int. J. Engines 8 (2015) 679–695.

[18] L. Cai, L. Kroger, H. Pitsch, Reduced and optimized mechanism for n-dodecane oxidation, in: 15th International Conference on Numerical Combustion, Vol. 4, 2015.

[19] T. Yao, Y. Pei, B.-J. Zhong, S. Som, T. Lu, K.H. Luo, A compact skeletal mechanism for n-dodecane with optimized semi-global low-temperature chemistry for diesel engine simulations, Fuel 191 (2017) 339–349.

[20] Sandia National Laboratories, Engine combustion network, 2024, https://ecn.sandia.gov/, (Accessed 29 July 2024).

[21] D. Jarrahbashi, S. Kim, B.W. Knox, C.L. Genzale, Computational analysis of end-of-injection transients and combustion recession, Int. J. Engine Res. 18 (2017) 1088–1110.

[22] X. Fang, R. Ismail, M.H. Davy, J. Camm, Numerical studies of combustion recession on ECN diesel Spray A, in: Internal Combustion Engine Division Fall Technical Conference, Vol. 51999, American Society of Mechanical Engineers, 2018, V002T06A011.

[23] P. Senecal, E. Pomraning, K. Richards, T. Briggs, C. Choi, R. McDavid, M. Patterson, Multi-dimensional modeling of direct-injection diesel spray liquid length and flame lift-off length using CFD and parallel detailed chemistry, SAE Trans. (2003) 1331–1351.

[24] Z. Gao, C. Jiang, C.-H. Lee, Representative interactive flamelet model and flamelet/progress variable model for supersonic combustion flows, Proc. Combust. Inst. 36 (2017) 2937–2946.

[25] J. van Oijen, A. Donini, R. Bastiaans, J. ten Thije Boonkkamp, L. de Goey, State-of-the-art in premixed combustion modeling using flamelet generated manifolds, Prog. Energy Combust. Sci. 57 (2016) 30–74.

[26] X. Fang, R. Ismail, M. Davy, A Study on Kinetic Mechanisms of Diesel Fuel Surrogate N-Dodecane for the Simulation of Combustion Recession, Tech. rep., SAE Technical Paper, 2019.

[27] Z. Luo, S. Som, S.M. Sarathy, M. Plomer, W.J. Pitz, D.E. Longman, T. Lu, Development and validation of an n-dodecane skeletal mechanism for spray combustion applications, Combust. Theor. Model. 18 (2014) 187–203.

[28] E. Ranzi, A. Frassoldati, A. Stagni, M. Pelucchi, A. Cuoci, T. Faravelli, Reduced kinetic schemes of complex reaction systems: fossil and biomass-derived transportation fuels, Int. J. Chem. Kinet. 46 (2014) 512–542.

[29] X.H. Fang, R. Ismail, K. Bushe, M. Davy, Simulation of ECN diesel Spray A using conditional source-term estimation, Combust. Theor. Model. 24 (2020) 725–760.

[30] M.M. Salehi, C. Devaud, W.K. Bushe, Advances and challenges of the Conditional Source-term Estimation model for turbulent reacting flows, Prog. Energy Combust. Sci. 104 (2024) 101172.

[31] X. Fang, N. Sekularac, M.H. Davy, Parametric studies of a novel combustion modelling approach for low temperature diesel spray simulation, in: Internal Combustion Engine Division Fall Technical Conference, Vol. 84034, American Society of Mechanical Engineers, 2020, V001T06A005.

[32] H. Pitsch, Large-eddy simulation of turbulent combustion, Annu. Rev. Fluid Mech. 38 (2006) 453–482.

[33] M. Zhang, J.C. Ong, K.M. Pang, X.-S. Bai, J.H. Walther, Large eddy simulation of transient combustion and soot recession in the ECN Spray A and D flames, Fuel 329 (2022) 125384.

[34] M. Zhang, J.C. Ong, K.M. Pang, S. Xu, Y. Zhang, A. Nemati, X.-S. Bai, J.H. Walther, Large eddy simulation of combustion recession: Effects of ambient temperature and injection pressure, Fuel 351 (2023) 128831.

[35] A. Yoshizawa, K. Horiuti, A statistically-derived subgrid-scale kinetic energy model for the large-eddy simulation of turbulent flows, J. Phys. Soc. Japan 54 (1985) 2834–2839.

[36] S. Menon, P.-K. Yeung, W.-W. Kim, Effect of subgrid models on the computed interscale energy transfer in isotropic turbulence, Comput. & Fluids 25 (1996) 165–180.

[37] X. Fang, Numerical Modelling for Diesel Spray Combustion (Ph.D. thesis), University of Oxford, 2019.

[38] S. Zhong, L. Xu, S. Xu, Y. Zhang, F. Zhang, K. Jiao, Z. Peng, X.-S. Bai, Assessment of grid/filter size dependence in large eddy simulation of high-pressure spray flames, Fuel 329 (2022) 125316.

[39] R.D. Reitz, R. Diwakar, Structure of high-pressure fuel sprays, SAE Trans. (1987) 492–509.

[40] J.C. Beale, R.D. Reitz, Modeling spray atomization with the Kelvin-Helmholtz/Rayleigh-Taylor hybrid model, At. Sprays 9 (1999).

[41] D.P. Schmidt, C.J. Rutland, A new droplet collision algorithm, J. Comput. Phys. 164 (2000) 62–80.

[42] A.A. Amsden, P.J. O'Rourke, T.D. Butler, KIVA-II: A Computer Program for Chemically Reactive Flows with Sprays, Tech. rep., Los Alamos National Lab.(LANL), Los Alamos, NM (United States), 1989.

[43] A.B. Liu, D. Mather, R.D. Reitz, Modeling the effects of drop drag and breakup on fuel sprays, SAE Trans. (1993) 83–95.

[44] J. Naber, R.D. Reitz, Modeling engine spray/wall impingement, SAE Trans. (1988) 118–140.

[45] M.A. Gonzalez D, G.L. Borman, R.D. Reitz, A study of diesel cold starting using both cycle analysis and multidimensional calculations, SAE Trans. (1991) 189–208.

[46] Convergent Science, Resolving turbulence-chemistry interactions in mixing-controlled combustion with LES and detailed chemistry, 2023, White Paper.

[47] Y. Pei, S. Som, E. Pomraning, P.K. Senecal, S.A. Skeen, J. Manin, L.M. Pickett, Large eddy simulation of a reacting spray flame with multiple realizations under compression ignition engine conditions, Combust. Flame 162 (2015) 4442–4455.

[48] Y. Pei, B. Hu, S. Som, Large-eddy simulation of an n-dodecane spray flame under different ambient oxygen conditions, J. Energy Res. Technol. 138 (2016) 032205.

[49] Y. Pei, E.R. Hawkes, S. Kook, G.M. Goldin, T. Lu, Modelling n-dodecane spray and combustion with the transported probability density function method, Combust. Flame 162 (2015) 2006–2019.

[50] S. Kim, J.I. Ryu, On the use of flamelet model approach in analyzing the mixing-controlled spray flame dynamics, Appl. Energy Combust. Sci. 17 (2024) 100234.

[51] T. Lu, C.S. Yoo, J. Chen, C.K. Law, Three-dimensional direct numerical simulation of a turbulent lifted hydrogen jet flame in heated coflow: a chemical explosive mode analysis, J. Fluid Mech. 652 (2010) 45–64.

[52] C. Xu, J.-W. Park, C.S. Yoo, J.H. Chen, T. Lu, Identification of premixed flame propagation modes using chemical explosive mode analysis, Proc. Combust. Inst. 37 (2019) 2407–2415.

[53] T. Lu, C. Yoo, J. Chen, The role of chemical explosive mode in flames, in: Fall Technical Meeting, the Eastern Section Meeting of the Combustion Institute, College Park, USA, 2009.

[54] S. Lai, S. Tang, C. Xu, N. Sekularac, X. Fang, Computational diagnostics for flame acceleration and transition to detonation in a hydrogen/air mixture, Combust. Flame 258 (2023) 113054.

[55] S. Lai, C. Xu, M. Davy, X. Fang, Flame acceleration and transition to detonation in a pre-/main-chamber combustion system, Phys. Fluids 34 (2022) 116105.

[56] T. Jaravel, O. Dounia, Q. Malé, O. Vermorel, Deflagration to detonation transition in fast flames and tracking with chemical explosive mode analysis, Proc. Combust. Inst. 38 (2021) 3529–3536.

[57] C. Xu, M.M. Ameen, S. Som, J.H. Chen, Z. Ren, T. Lu, Dynamic adaptive combustion modeling of spray flames based on chemical explosive mode analysis, Combust. Flame 195 (2018) 30–39.

[58] S. Zhong, S. Xu, F. Zhang, Z. Peng, L. Chen, X.-S. Bai, Cool flame wave propagation in high-pressure spray flames, Proc. Combust. Inst. 39 (2023) 2513–2522.
[59] M. Gadalla, S. Karimkashi, I. Kabil, O. Kaario, T. Lu, V. Vuorinen, Embedded direct numerical simulation of ignition kernel evolution and flame initiation in dual-fuel spray assisted combustion, Combust. Flame 259 (2024) 113172.
[60] J.M. Desantes, J.J. López, J.M. García-Oliver, D. López-Pintor, Experimental validation and analysis of seven different chemical kinetic mechanisms for n-dodecane using a rapid compression-expansion machine, Combust. Flame 182 (2017) 76–89.
[61] C. Gong, M. Jangi, X.-S. Bai, Large eddy simulation of n-dodecane spray combustion in a high pressure combustion vessel, Appl. Energy 136 (2014) 373–381.
[62] S. Farjam, B. Savard, Ignition and flame stabilization of n-dodecane turbulent premixed flames under Spray A thermochemical conditions, Combust. Flame 242 (2022) 112133.
[63] T. Zhou, P. Zhao, T. Ye, M. Zhu, C. Tao, Direct numerical simulation of low temperature reactions affecting n-dodecane spray autoignition, Fuel 280 (2020) 118453.
[64] D.K. Dalakoti, B. Savard, E.R. Hawkes, A. Wehrfritz, H. Wang, M.S. Day, J.B. Bell, Direct numerical simulation of a spatially developing n-dodecane jet flame under Spray A thermochemical conditions: Flame structure and stabilisation mechanism, Combust. Flame 217 (2020) 57–76.
[65] A. Krisman, E.R. Hawkes, J.H. Chen, Two-stage autoignition and edge flames in a high pressure turbulent jet, J. Fluid Mech. 824 (2017) 5–41.
[66] G. Borghesi, A. Krisman, T. Lu, J.H. Chen, Direct numerical simulation of a temporally evolving air/n-dodecane jet at low-temperature diesel-relevant conditions, Combust. Flame 195 (2018) 183–202.
[67] M. Sitte, C. Turquand d'Auzay, A. Giusti, E. Mastorakos, N. Chakraborty, A-priori validation of scalar dissipation rate models for turbulent non-premixed flames, Flow Turbul. Combust. 107 (2021) 201–218.
[68] E. Mastorakos, Ignition of turbulent non-premixed flames, Prog. Energy Combust. Sci. 35 (2009) 57–97.
[69] H. Bao, N. Maes, H.Y. Akargun, B. Somers, Large eddy simulation of cavitation effects on reacting spray flames using FGM and a new dispersion model with multiple realizations, Combust. Flame 236 (2022) 111764.
[70] C.K. Blomberg, L. Zeugin, S.S. Pandurangi, M. Bolla, K. Boulouchos, Y.M. Wright, Modeling split injections of ECN "Spray A" using a conditional moment closure combustion model with RANS and LES, SAE Int. J. Engines 9 (2016) 2107–2119.